MRI biomarkers in neuro-oncology

Marion Smits

Abstract | The central role of MRI in neuro-oncology is undisputed. The technique is used, both in clinical practice and in clinical trials, to diagnose and monitor disease activity, support treatment decision-making, guide the use of focused treatments and determine response to treatment. Despite recent substantial advances in imaging technology and image analysis techniques, clinical MRI is still primarily used for the qualitative subjective interpretation of macrostructural features, as opposed to quantitative analyses that take into consideration multiple pathophysiological features. However, the field of quantitative imaging and imaging biomarker development is maturing. The European Imaging Biomarkers Alliance (EIBALL) and Quantitative Imaging Biomarkers Alliance (QIBA) are setting standards for biomarker development, validation and implementation, as well as promoting the use of quantitative imaging and imaging biomarkers by demonstrating their clinical value. In parallel, advanced imaging techniques are reaching the clinical arena, providing quantitative, commonly physiological imaging parameters that are driving the discovery, validation and implementation of quantitative imaging and imaging biomarkers in the clinical routine. Additionally, computational analysis techniques are increasingly being used in the research setting to convert medical images into objective high-dimensional data and define radiomic signatures of disease states. Here, I review the definition and current state of MRI biomarkers in neuro-oncology, and discuss the clinical potential of quantitative image analysis techniques.

The insight that survival, response to treatment and toxicity of treatment varies widely among patients with the same general tumour type has led to the tailoring of brain tumour management to individual patient characteristics — known as precision medicine. This approach has resulted in an exponential increase in the complexity of diagnosis and choice of therapeutic strategy, both of which are now informed by many clinical, pathological and genetic factors. In parallel, an expansion in the amount of imaging data available and a diversification of information content has enabled in vivo tumour assessment to extend well-beyond traditional macrostructural image interpretation. The development of imaging biomarkers, which requires quantitative image acquisition and analysis, now offers the opportunity to move precision diagnostics forward. Both imaging biomarkers and computational imaging approaches have the potential to influence cancer outcomes by elucidating the 3D morphology and biology of tumours from information-rich imaging modalities, thus enabling radiologists to correlate structural information with functional information on the cellular level.

These developments in neuroimaging are particularly relevant to glioma, given the recent insights into the importance of molecular differences between histopathologically similar tumours[1]. This relevance is reflected in the published literature on neuro-oncological imaging biomarkers, which is much more abundant for glioma than for other neuro-oncological entities such as brain metastasis and meningioma. The current WHO classification of CNS tumours distinguishes three main categories of adult diffuse glioma on the basis of mutation of the isocitrate dehydrogenase (IDH) gene and co-deletion of chromosome arms 1 and 19 (1p/19q co-deletion)[2]. These categories are: *IDH*-mutated 1p/19q non-co-deleted (*IDH*-mut astrocytoma), *IDH*-mut 1p/19q co-deleted (oligodendroglioma), and *IDH*-wild-type (*IDH*-wt glioma) tumours. *IDH*-mutated tumours are associated with a much more favourable prognosis than tumours of similar lineage and grade that are *IDH*-wt[3]. The categorization of tumours by *IDH* and 1p/19q co-deletion genotype is based on tissue obtained through surgery, but predicting these genotypes from imaging phenotypes prior to surgery can aid medical decision-making[4]. These kinds of predictions are still limited to the research arena, but they are particularly important, as it is increasingly recognized that treatment response is determined by multiple extrinsic and intrinsic factors, including tumour genotype. Similarly, brain metastases can display heterogeneous characteristics even within an individual patient. In this context, non-invasive imaging biomarkers have the

Department of Radiology & Nuclear Medicine, Erasmus MC, University Medical Centre Rotterdam, Rotterdam, Netherlands.

e-mail: marion.smits@erasmusmc.nl

https://doi.org/10.1038/s41582-021-00510-y

Key points

- Imaging biomarkers offer the opportunity to move precision diagnostics forward, enabling better informed medical decision-making and tracking of biological changes before, during and after brain tumour treatment.
- Guidelines and standards for data acquisition, image processing and validation processes for the development and eventual implementation of imaging biomarkers are provided by the European Society of Radiology and the Radiological Society of North America.
- Radiomics is a rapidly emerging field of imaging research delivering an almost limitless supply of potential imaging biomarkers for improved patient and disease characterization.
- The currently available evidence on imaging biomarkers and radiomics is still mostly at the discovery level; rigorous technical, biological and clinical validation are needed for clinical application.

potential not only to track biological changes during or after treatment, but also to predict response prior to or early after treatment. Another important application of imaging biomarkers is in the differentiation of treatment-related abnormalities from tumour progression. Treatment-related abnormalities, including pseudoprogression and radiation necrosis, look very similar to true tumour progression on conventional MRI; however, imaging biomarkers derived from advanced MRI techniques are better able to differentiate between these entities.

In this Review, I address the definition and current state of MRI biomarkers in neuro-oncology, and discuss the quantitative image analysis techniques that hold clinical potential. The focus of this paper is MRI, as this is the most commonly used imaging technique in neuro-oncology; however, it should be noted that radionuclide imaging with PET is increasingly used to supplement MRI in the clinical management of glioma[5], meningioma[6] and brain metastasis[7].

Imaging biomarkers

Biomarkers constitute a broad category of objective indicators of a healthy or disease state that should be measurable, precise, accurate and true[8,9]. Although the value of biomarkers in both research and clinical practice is undisputed, clinical implementation of imaging biomarkers is far from commonplace. This sparsity can, in part, be attributed to a lack of rigorous biomarker evaluation, which has resulted in the almost non-existent regulatory qualification of imaging biomarkers. Conceptually, the requirements for imaging biomarkers (as specified below) are no different from those for biomarkers that are based on laboratory assays, but these are not trivial to meet, as the imaging field does not have a tradition of standardization across image acquisition, reconstruction or post-processing approaches. These challenges do not mean that the requirements should be abandoned, but it is important that they are operationalized for this specific field of research and development. A roadmap towards achieving this aim was developed for the cancer field by the European Organisation for Research and Treatment of Cancer (EORTC) and Cancer Research UK, and published in 2017 (REF.[10]). The roadmap provided 14 recommendations for the acceleration of imaging biomarker development that spanned grant submissions, study publications, validation (technical, biological and clinical) and qualification.

More generally, the advancement of imaging biomarkers in radiology is driven by its two major societies, the European Society of Radiology (ESR) and the Radiological Society of North America (RSNA). ESR's European Imaging Biomarkers Alliance (EIBALL) and RSNA's Quantitative Imaging Biomarkers Alliance (QIBA) collaborate closely, with the aim of providing guidelines and setting standards for data acquisition and image processing, as well as the validation processes that are necessary for the development and eventual implementation of imaging biomarkers in clinical practice and clinical trials. Although outside the scope of this Review, it should be noted that similar activities have been undertaken in the field of nuclear medicine. An important effort was the publication of joint practice guidelines for glioma imaging using PET with radiolabelled amino acids and fluorodeoxyglucose by the European Association of Nuclear Medicine, the Society of Nuclear Medicine and Molecular Imaging, the European Association of Neuro-Oncology, and the Response Assessment in Neuro-oncology (RANO) PET working group[11]. QIBA also provides guidance on PET-derived biomarkers, but this guidance does not cover neuro-oncological applications.

Imaging biomarker requirements

Precision, trueness and accuracy. One of the first steps in the development and implementation of imaging biomarkers will be the correct and consistent use of internationally standardized and accepted terminology and definitions[8,12]. For biomarkers to be objective and reproducible, they should be precise, accurate and true. In this context, 'precision' refers to the variability in the measurements and constitutes both repeatability and reproducibility. Potential sources of variability include the clinical population, image acquisition, reconstruction and post-processing, as well as the measurement methodology. These sources should be explicitly identified prior to analysis and reported in publications[8]. 'Trueness' refers to how close the measurement is to a true, or reference, value. For quantitative imaging biomarkers, trueness can be estimated, with a phantom providing reference values; however, physical measurements come with a certain inherent error and thus the 'true' value can never be known with certainty[12]. 'Accuracy' has multiple meanings, sometimes referring to the level of bias, but in the context of imaging biomarkers the term is used to designate how well a test performs in a clinical setting in terms of sensitivity, specificity and area under the receiver operating characteristic curve (AUC).

Imaging biomarker validation. For the typical, biologically determined imaging biomarker, the validation process consists of consecutive technical (performance), biological and clinical (end point) validation[13,14]. This validation process follows the discovery phase, in which an imaging biomarker with a known relationship to the underlying biological process is identified. For technical validation, data are collected using standardized acquisition protocols in a limited number of expert centres,

Repeatability
The frequency with which the same measurement under the same conditions (for example, same scanner, participant and rater) provides the same result.

Reproducibility
The frequency with which the same measurement performed under different conditions (for example, on a different scanner or by a different rater) provides the same result.

Phantom
An artificial construct, either physical or digital, that provides a reference standard for validation and calibration.

Sensitivity
The proportion results from a given test that are true positives.

Specificity
The proportion results from a given test that are true negatives.

Brownian motion
The random motion of particles within a medium.

Ki-67 labelling index
A marker of cellular proliferation based on immunohistochemical assessment of the expression of the Ki-67 protein.

to establish that the biomarker can be reliably obtained under a variety of common conditions (for example, across various widely applied image acquisition platforms). This technical validation is combined with an assessment of the biomarker's biological validity; for example, correlation of the imaging biomarker values with histopathological tissue features. If technical and biological validation is successful, the biomarker can then be validated in a clinical setting against a specific reference standard — in independent cohorts and in a multicentre, prospective trial setting — to establish the unambiguous relationship between the biomarker and the clinical end point.

An alternative approach to imaging biomarker development is to begin the discovery phase with a large data set, from which candidate biomarkers are identified[14]. With this approach, biological validation is not mandatory, as such a data-driven approach could find associations between imaging markers and disease states for which the underlying disease process is not yet established. If this occurs, a biological link can be explored a posteriori[14].

Regulatory standards and qualification

As yet, regulatory bodies for imaging biomarkers are lacking, and routine quality assurance and control procedures do not exist. Therefore, thresholds for biomarker acceptance are left to the discretion of the professional community. To mitigate the risk of poorly validated imaging biomarkers entering clinical practice, the ESR has proposed minimum criteria[15] inspired by the guideline on bioanalytical method validation from the European Medicines Agency[16,17]. Regarding precision, the ESR criteria require a coefficient of variation (CoV) of <15%, except when measurements are below the lowest limit of quantification (LLoQ); in these cases a CoV of ≤20% is acceptable[15]. In terms of assessing bias, for example, by use of a phantom or biological reference value, the criteria require the standard error to be <15%, which can be relaxed to ≤20% if measurements are below the LLoQ. Finally, for clinical validation, an AUC (that is, diagnostic accuracy) of >0.85 is required.

The QIBA approach is to use the known measurement error as a threshold beyond which differences between two longitudinal measurements can be confidently attributed to true change[18]. These QIBA biomarker thresholds, or 'claims', are available on the QIBA wiki together with the procedures needed to reach the required level of measurement accuracy, referred to as 'profiles'[19]. When publishing the results of imaging biomarker quantification, the context of the assessment should be described (for example, the clinical population or indication) such that it is explicitly clear how to use and interpret the value of a particular biomarker.

Quantitative imaging

Quantitative imaging is a fundamental aspect of imaging biomarker development[20]. QIBA defines quantitative imaging as the "extraction of quantifiable features from medical images for the assessment of normal or the severity, degree of change, or status of a disease, injury, or chronic condition relative to normal"[12]. In a 2021 survey on the use of quantitative MRI in clinical practice in Europe, the most commonly used quantitative imaging techniques in clinical neuroradiological practice were diffusion MRI (dMRI; used by 82% of respondents), perfusion MRI (pMRI; used by 67% of respondents) and MR spectroscopy (MRS; used by 64% of respondents)[21].

Quantitative MRI in neuro-oncology

MRI is the workhorse of brain tumour imaging. Conventional MRI, such as T1-weighted and T2-weighed sequences, provide macrostructural anatomical information, whereas advanced MRI techniques (for example, dMRI, pMRI and MRS) are more sensitive and/or specific to biophysical, cellular and microstructural processes. These advanced techniques are also potentially (semi)quantitative, in contrast to conventional MRI techniques, which only provide relative image contrasts. Sensitivity, specificity and quantification are important for imaging biomarker acquisition.

Diffusion MRI

Apparent diffusion coefficient. dMRI is widely used in neuro-oncology, although rarely quantitatively. A European-wide survey found that maps of the apparent diffusion coefficient (ADC) — the most commonly used dMRI metric — were overwhelmingly used qualitatively (78% of respondents), by visual inspection only[22]. To my knowledge, a 2020 guideline for response assessment in paediatric high-grade glioma is the first and only clinical neuro-oncology guideline to include advanced MRI, that is, dMRI, in its response criteria — albeit only qualitatitively[23].

dMRI measures the displacement of free water molecules resulting from Brownian motion (FIG. 1) and the ADC is a measure of the magnitude of diffusion. ADC is considered to be a surrogate marker of cellular density[24,25] and was inversely correlated with the Ki-67 labelling index in a retrospective study of high-grade astrocytoma[26]. Information on the accuracy and precision of ADC measurement in the brain is scarce. The QIBA consensus profile of diffusion-weighted imaging states that a longitudinal difference of ≥11% can be attributed to true change[27]. This figure is based on the results of three test–retest studies[28–30].

ADC findings in various neuro-oncological scenarios are variable and commonly conflicting[24,31]. In addition to technical and methodological variations, this variability is probably in large part a result of underlying tumour heterogeneity. Compared with lower-grade brain tumours, higher-grade brain tumours display higher degrees of cellularity, with low ADC; however, they also display higher degrees of necrosis and vasogenic oedema, with high ADC[24,31]. One way to account for such tumour heterogeneity is to calculate the proportion of tumour with ADC values above a certain threshold, such that subregions of the tumour with high ADC can be separately identified; in one study the proportion of the tumour consisting of this high-ADC subregion correlated well with glioma genotype[32].

Despite the variability, the literature supporting the potential of ADC as an imaging biomarker is abundant.

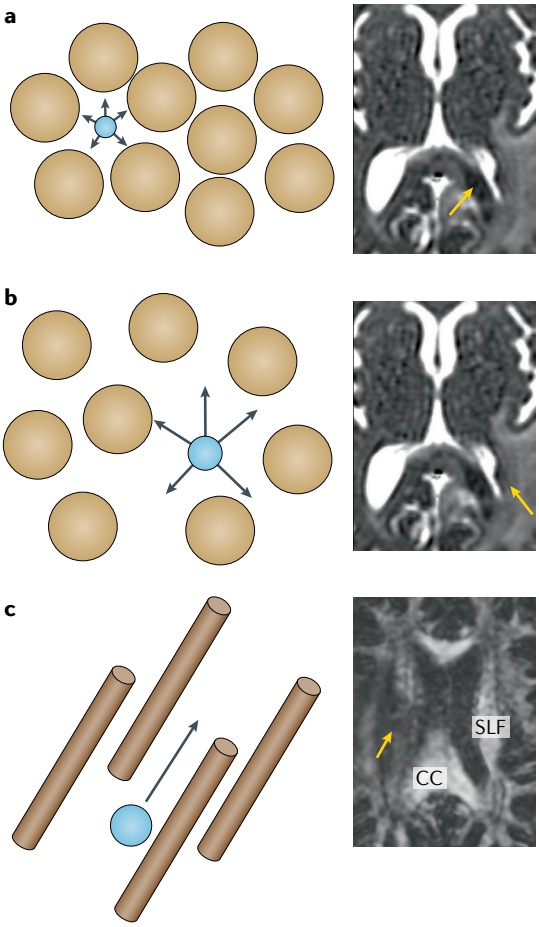

Fig. 1 | **Diffusion MRI. a** | Increased cellular density reduces the extracellular space, thus reducing the diffusion of water through the tissue. This effect is exemplified in a patient with a left parietal glioblastoma extending into the splenium. An area of low signal intensity (yellow arrow), consistent with a low apparent diffusion coefficient (ADC), can be observed at the location of the tumour. **b** | Vasogenic oedema increases the extracellular space, enabling water to diffuse further through the tissue and increasing the ADC. An area of high signal intensity (yellow arrow) can be seen at the site of oedema. **c** | The preferential diffusion of water along white matter tracts is detected by diffusion MRI as an increase in fractional anisotropy (FA). The effect of a brain tumour on FA is exemplified in a patient with right frontal glioblastoma (yellow arrow) extending into the superior longitudinal fasciculus (SLF). The healthy, left SLF can be seen as an area of high signal intensity; however, the right SLF has been infiltrated by the tumour and has a much lower FA. CC, corpus callosum.

Various meta-analyses have found that ADC can be used to differentiate between high-grade and low-grade glioma (in both adult patients[33,34] and paediatric patients[35]), between high-grade glioma and brain metastasis[36], and between tumour progression and treatment-related abnormalities[37,38] (TABLE 1). Meta-analyses have also found that ADC findings can be used to predict survival[39] and *IDH* mutation status[40]. Furthermore, in several separate studies, of which no meta-analysis is available, ADC was found to correlate with survival in individuals with diffuse infiltrative pontine glioma, irrespective of H3K27M status[41–43] (H3K27M is the most common mutation in this type of tumour). The overall finding from this area of research is that lower ADC is associated with higher tumour grade, tumour progression, poorer survival and unfavourable genotype (*IDH*-wt).

Fractional anisotropy. In addition to assessing the ADC, dMRI can also be extended to assess the directionality of diffusion, providing a measure of fractional anisotropy (FA). FA ranges from 0 to 1, where 0 represents equal diffusion in all directions, and 1 represents diffusion in a single direction only (FIG. 1). In several studies, FA was higher in *IDH*-wt than in *IDH*-mut glioma, but tumour diagnosis on the basis of FA was no more accurate than diagnosis on the basis of ADC[31,44,45]. A meta-analysis found FA in the tumour core to be greater in high-grade glioma than in low-grade glioma (21 studies, 734 participants); the reverse was observed in the periphery of the tumour (7 studies, 180 participants), suggesting that high-grade glioma are more destructive of the perifocal white matter[46]. However, the observed differences in FA (pooled average, 0.02) between high-grade and low-grade glioma seem to be too small for meaningful use. According to another meta-analysis (9 studies, 344 participants), differences in FA between high-grade glioma and brain metastasis were also found to be too small to be diagnostically useful — only the peritumoural region of high-grade glioma had a significantly higher FA than metastasis[47]. This divergence is presumably a result of the differences between the infiltrative oedema of glioma and the vasogenic oedema that surrounds metastasis[24].

Other dMRI techniques. Diffusion kurtosis imaging, an advanced form of dMRI, is more sensitive to microstructural tissue changes — most commonly expressed as mean kurtosis — than traditional dMRI techniques[48]. Other advanced dMRI approaches include neurite orientation dispersion and density imaging (NODDI)[49] and vascular, extracellular and restricted diffusion for cytometry in tumours (VERDICT)[50]. Both of these approaches use biophysiological models as a priori knowledge to enable more detailed assessment of tissue microstructure; NODDI is primarily modelled on healthy brain tissue[49] and VERDICT was originally optimized for prostate cancer imaging[50], but has now also been applied to brain tumours[51]. Intravoxel incoherent motion (IVIM)[52] is a technique on the boundary of diffusion and perfusion imaging; it analyses the measured diffusion component that results from the slow flow of blood in the capillaries — the so-called microvascular fraction.

Compared with FA, mean kurtosis is thought to better represent the restricted component in biological tissue and seems to hold more promise for differentiating between high-grade and low-grade glioma, as indicated by the results of two meta-analyses including 619 and 430 participants from nine and ten studies, respectively[48,53] (TABLE 1). Similarly, a meta-analysis of nine IVIM studies (318 participants) identified an increase in perfusion coefficient — as well as a reduction in ADC and diffusion coefficient — in high-grade

Mean kurtosis
An estimate of the non-gaussianity of water diffusion resulting from the presence of diffusion barriers and compartments within tissue structure; higher mean kurtosis indicates higher tissue microstructural complexity.

glioma compared with low-grade glioma[54] (TABLE 1). However, both mean kurtosis and IVIM are challenging techniques to perform and are not widely available.

Data on the utility of NODDI and VERDICT as neuro-oncological biomarkers are extremely limited. In a prospective study using NODDI, extracellular volume fraction in the peritumoural region was shown to distinguish solitary brain metastasis ($n=6$) from glioblastoma ($n=9$), presumably as a result of the differences between infiltrative and vasogenic oedema mentioned above[55]. In a study of the ability of VERDICT to assess glioma microstructure, a significant difference in the volume of the intracellular compartment between *IDH*-mut ($n=7$) and *IDH*-wt ($n=7$) glioma was observed, even when no difference in ADC was detected[51].

Perfusion MRI

Relative cerebral blood volume. pMRI is used widely in neuro-oncology and relies on the detection of differences in (neo)vascularization between normal and neoplastic tissue, as well as between different types of neoplasia. In current clinical practice, ~50% of users apply pMRI quantitatively[22]. Three main pMRI techniques exist, of which dynamic susceptibility contrast (DSC) pMRI is by far the most commonly used[21,22] (FIG. 2). This technique is based on the capture of the signal change that occurs during the passage of a bolus of intravenously administered contrast agent through the brain. DSC pMRI provides a semiquantitative estimate of relative cerebral blood volume (rCBV), which is usually measured as a ratio between the tumour and the contralateral

Table 1 | **Meta-analyses of diffusion MRI studies in neuro-oncology**

Meta-analysis	Number of studies (number of participants)	Metric (number of studies)	Threshold (range)[a]	AUC (95% CI)	Sensitivity (95% CI)	Specificity (95% CI)	Other
Distinguishing high-grade glioma from low-grade glioma							
Hales et al. (2019)[35]	9 (290)[b]	ADC_{mean}	0.95[c] (0.9–1.21)	NA	NA	NA	Accuracy 96%[d]
		ADC_{min}	0.82[c] (0.82–0.96)	NA	NA	NA	Accuracy 83%[d]
Zhang et al. (2017)[33]	15 (821)[f]	Absolute ADC (12), ratio (3)	NA	0.90	0.85 (0.80–0.90)	0.80 (0.71–0.87)	NA
Wang et al. (2020)[34]	18 (1,172)[f]	ADC_{min} (8)	0.216–1.60; 0.70–1.252; 0.86–1.50	0.91 (0.88–0.93)	0.81 (0.75–0.86)	0.87 (0.81–0.91)	NA
Miloushev et al. (2015)[46]	17 (772)[f]	MD_{min}	0.98[e]	0.84 (0.76–0.91)	78% (67–88%)	78% (64–89%)	NA
Falk Delgado et al. (2018)[53]	10 (430)[g]	Mean kurtosis	NA	0.94	0.85 (0.74–0.92)	0.92 (0.81–0.96)	NA
Abdalla et al. (2020)[48]	9 (619)[g]	Mean kurtosis	0.5–0.6	0.87	0.85	0.92	NA
Li et al. (2018)[54]	9 (318: 185 HGG and 133 LGG)	ADC, D, D*	NA	NA	NA	NA	D lower and D* higher in HGG
Prediction of survival (irrespective of tumour grade)							
Zulfiqar et al. (2013)[39]	4 (181)	ADC_{min}	0.6–1.0	NA	NA	NA	Odds ratio 12.44
Prediction of IDH mutation status							
Suh et al. (2019)[40]	8 (823: 95 with and 728 without *IDH* mutation)	ADC/PWI	NA	NA	84% (75–94%)	87% (78–97%)	NA
Distinguishing solitary metastasis from HGG							
Suh et al. (2018)[36]	14 (1,143: 640 HGG and 503 metastasis)	ADC (7), FA (7), MD (5)	Wide variation	NA	80% (71–86%)	81% (80–84%)	NA
Jiang et al. (2014)[47]	9 (344: 193 HGG and 151 metastasis)	FA, MD	NA	NA	NA	NA	Only peritumoural differences
Distinguishing glioma recurrence from treatment-related abnormalities							
Yu et al. (2020)[37]	3 (129)	ADC_{mean}	1.2–1.6	0.94	0.95 (0.89–0.98)	0.83 (0.72–0.91)	NA
	1 (35)	Relative ADC	0.25				
	2 (50)	5th percentile	0.84–0.91				
van Dijken et al. (2017)[38]	7 (204 HGG)	ADC	NA	NA	71% (60– 80%)	87% (77–93%)	NA

ADC, apparent diffusion coefficient; AUC, area under the receiver operating characteristic curve; D, diffusion coefficient; D*, perfusion coefficient; FA, fractional anisotropy; HGG, high-grade glioma, IDH, isocitrate dehydrogenase; LGG, low-grade glioma, MD, mean diffusivity; NA, not available; PWI, perfusion weighted imaging. [a]In 10^{-3} mm^2/s unless ratio. [b]Paediatric, diffuse midline glioma excluded. [c]Threshold derived from own independent cohort ($n=25$), range from literature. [d]Accuracy based on optimal threshold derived from own cohort. [e]Determined from individual patient data ($n=105$). [f,g]Meta-analyses that include some of the same studies.

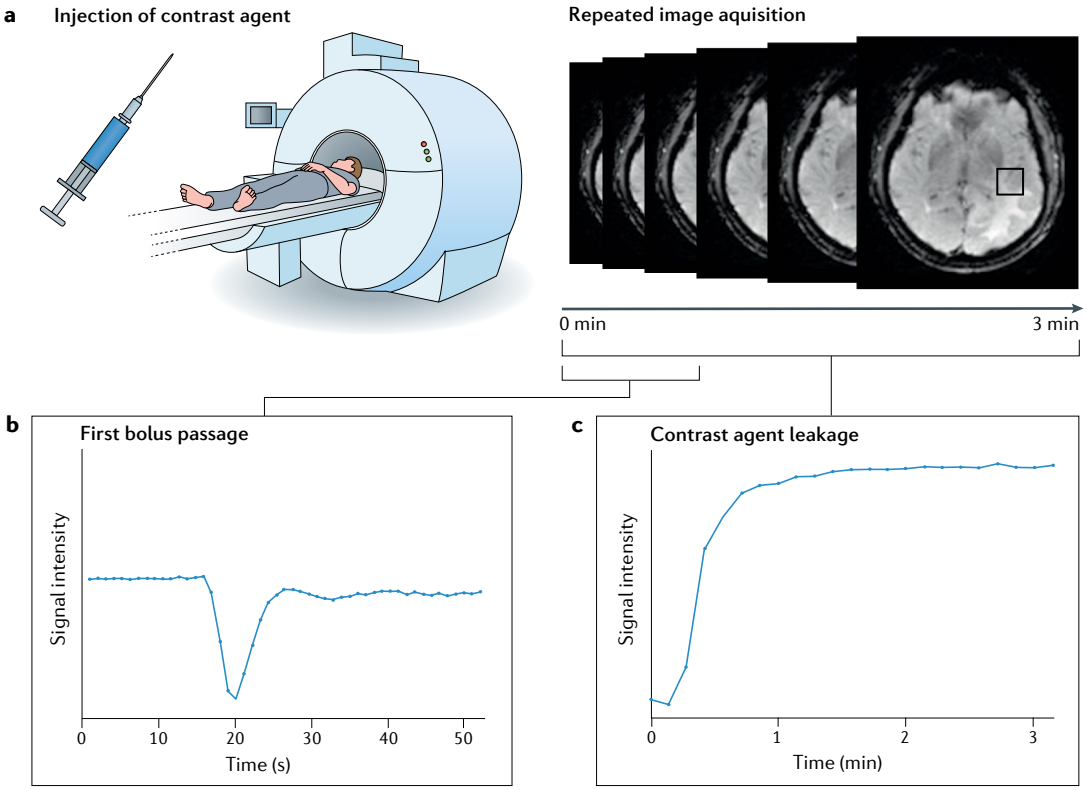

Fig. 2 | **Perfusion MRI. a** | For perfusion MRI, a contrast agent is administered by intravenous injection. Administration is followed by repeated image acquisition and the signal intensity is plotted for each pixel in the brain (black square; ~3 × 3 mm^2). **b** | Dynamic susceptibility contrast perfusion MRI captures the first passage of the contrast agent bolus through the brain vasculature with a series of fast scans — one scan per <1.5 s — resulting in the signal intensity curve, which can be used to estimate the cerebral blood volume for each pixel. **c** | Dynamic contrast-enhanced scanning also follows the intravenous administration of contrast agent, but measures the signal intensity in the brain parenchyma during a prolonged period of time (>5 min) to plot the leakage of contrast agent across the blood–brain barrier (K^{trans}).

normal-appearing white matter. Despite extensive use of DSC pMRI in clinical practice, no broad consensus has been reached on acquisition technique, post-processing algorithms, analysis or interpretation. This lack of consensus has severely hampered application of DSC pMRI as an imaging biomarker thus far.

Two studies used pMRI to guide stereotactic glioma biopsies and showed that rCBV correlates with vessel density, endothelial proliferation and tumour grade[56,57]. In another study, the repeatability and reproducibility of rCBV assessment of recurrent glioma were found to be moderate (49.5% and 5.5%, respectively)[58]. In terms of acquisition, high reliability and reproducibility have been reported for various DSC approaches[59–62]. Several studies have shown that differences in software or applied algorithms are a large source of variability in measured rCBV values[62–64]. At present, the QIBA profile for DSC-MRI does not provide a claim for rCBV, owing to a lack of supporting literature[65].

Indeed, the extensive literature on rCBV in neuro-oncology provides a wide range of cut-off values for each of the various clinical indications for which pMRI is used, but no uniform threshold values have been established (TABLE 2). The available meta-analyses, which include data on glioma and brain metastasis, indicate that rCBV is higher in tumours of higher grade[66,67] or higher aggressiveness (defined by *IDH* genotype)[40,68], and that rCBV is higher in areas of tumour recurrence than in treatment-related abnormalities[38,69–71]. Although the overall reported accuracies for glioma grading are good — an AUC of 0.77 (REF.[66]), and pooled sensitivity and specificity of 0.83 and 0.48, respectively[67] — accuracy is very much influenced by the type of tumour. Glioma with the *IDH*-mut 1p/19q co-deleted genotype (oligodendroglioma) display internal vascularization, which results in mildly elevated perfusion, even at a low grade[72]. This cross-confounding effect of *IDH*, and particularly 1p/19q, status with tumour grade on perfusion — as well as diffusion — parameters is important to keep in mind when appreciating the performance of these imaging biomarkers. Indeed, in two meta-analyses, subgroup analyses showed that rCBV has a much lower accuracy for grading oligodendroglioma than for grading astrocytoma[66,67].

According to a meta-analysis of 18 studies (900 participants), peritumoural rCBV is better than intratumoural rCBV at differentiating between brain metastasis and high-grade glioma[73] (TABLE 2). In the peritumoural region, rCBV was higher in high-grade glioma than in metastasis, presumably owing to (microscopic) tumour infiltration. Another meta-analysis assessed the ability of various pMRI techniques to differentiate high-grade

Table 2 | **Meta-analyses of perfusion MRI studies in neuro-oncology**

Meta-analysis	Number of studies (number of participants)	Technique and metric (number of studies)	Threshold	AUC (95% CI)	Sensitivity (95% CI)	Specificity (95% CI)	Other
Distinguishing HGG from LGG							
Delgado and Delgado (2017)[f,66]	28 (727)	DSC: rCBV ratio	2.0[a]	0.77	NA	NA	Only grade II and grade III
Abrigo et al. (2018)[f,67]	7 (115 non-enhancing glioma: 83 LGG and 32 HGG)	DSC: rCBV ratio	1.75[b]	NA	0.83 (0.66–0.93)	0.48 (0.09–0.90)	Average rCBV ratio 1.29 (0.01–5.10) in LGG, 1.89 (0.30–6.51) in HGG
Hales et al. (2019)[35]	5 (252 paediatric)	ASL: $nCBF_{max}$	1.45 (0.94–1.52)	NA	NA	NA	Accuracy 83%[c]
Okuchi et al. (2019)[79]	14 (546: 356 HGG and 190 LGG)	DCE, K^{trans} mostly used, hot-spot most accurate	NA	0.96	0.93	0.90	NA
Kong et al. (2017)[82]	9 (305: 197 HGG and 108 LGG)	ASL: CBF absolute and CBF ratio	NA	NA	NA	NA	Higher values in HGG than in LGG
Distinguishing tumour (glioma, brain metastasis) recurrence from treatment-related abnormalities							
Chuang et al. (2016)[g,69]	10[d] (325: 228 TP and 97 TRA)	DSC: rCBV ratio	1.73–6.71	NA	NA	NA	NA
Wang et al. (2020)[g,70]	20 (939 HGG)	DSC[e]	0.71–4.06	0.89	0.83 (0.79–0.86)	0.83 (0.78–0.87)	NA
	4 (252 HGG)	DCE[e]	NA	0.94	0.73 (0.66–0.80)	0.80 (0.69–0.88)	NA
	3 (160 HGG)	ASL[e]	NA	0.88	0.79 (0.69–0.87)	0.78 (0.67–0.87)	NA
van Dijken et al. (2017)[g,38]	18 (708 HGG)	DSC	NA	NA	87% (82–91%)	86% (77–91%)	NA
	5 (207 HGG)	DCE	NA	NA	92% (73– 98%)	85% (76–92%)	NA
	2 (102 HGG)	ASL	NA	NA	5–79%	64–82%	NA
Patel et al. (2017)[g,71]	20 (1,455 HGG)	DSC: $rCBV\ ratio_{mean}$	0.9–2.15	NA	88% (0.81–0.94)	88% (0.78– 0.95)	NA
		DSC: $rCBV\ ratio_{max}$	1.49–3.1	NA	93% 0.86–0.98)	75% (0.66–0.85)	NA
	11 (581 HGG)	DCE[e]	NA	NA	89% (0.78–0.96)	85% (0.77–0.91)	NA
Okuchi et al. (2019)[g,79]	9 (298: 179 TP and 119 TRA)	DCE, K^{trans} mostly used, hot-spot most accurate	NA	0.89	0.88	0.86	NA
Distinguishing solitary metastasis from HGG							
Suh et al. (2018)[73]	18 (900: 542 HGG and 358 metastasis)	pMRI (DSC, DCE or ASL)	Variable	0.96 (0.94–0.98)	0.90 (0.84–0.94)	0.91 (0.84–0.95)	NA
	Subgroup analysis of 10 studies (441: 260 HGG and 181 metastasis)	DSC: peritumoural rCBV	0.5–1.7 (median 1.2)	NA	0.89 (0.80–0.94)	0.88 (0.74–0.95)	NA
	Subgroup analysis of 3 studies (222: 148 HGG and 74 metastasis)	ASL: peritumoural rCBF	0.4–1.1	NA	0.81 (0.60–1.0)	0.93 (0.82–1.0)	NA
Distinguishing HGG from PCNSL							
Okuchi et al. (2019)[79]	5 (224: 68 PCNSL and 156 HGG)	DCE, K^{trans} mostly used, hot-spot most accurate	NA	0.86	0.78	0.81	NA
Xu et al. (2017)[74]	14 (598: 178 PCNSL and 420 HGG)	pMRI overall	Variable	0.94	0.88 (0.85–0.91)	0.84 (0.78–0.89)	Best-performing metric per study
		DSC (6)	Variable	0.98	0.96 (0.92–0.99)	0.86 (0.77–0.93)	
		ASL (5)	Variable	0.94	0.83 (0.75–0.89)	0.90 (0.78–0.96)	
		DCE (3)	Variable	0.92	0.88 (0.81–0.94)	0.76 (0.61–0.87)	
		IVIM (2)	Variable	NA	NA	NA	

Table 2 (cont.) | **Meta-analyses of perfusion MRI studies in neuro-oncology**

Meta-analysis	Number of studies (number of participants)	Technique and metric (number of studies)	Threshold	AUC (95% CI)	Sensitivity (95% CI)	Specificity (95% CI)	Other
Predicting response to bevacizumab treatment in recurrent glioblastoma							
Choi et al. (2016)[75]	4 on PFS (226), 5 on OS (247)	DSC: change in rCBV, post-treatment rCBV (maximum, mean or median)	NA	NA	NA	NA	Pooled HR for responders: 0.46 (0.28–0.76) for PFS, 0.47 (0.29–0.76) for OS

ASL, arterial spin labelling; AUC, area under the receiver operating characteristic curve; DSC, dynamic susceptibility contrast; DCE, dynamic contrast-enhanced; HGG, high-grade glioma; IVIM, intravoxel incoherent motion; K^{trans}, volume transfer constant; LGG, low-grade glioma; NA, not available; $nCBF_{max}$, maximum cerebral blood flow normalized to contralateral grey matter[35]; OS, overall survival; PCNSL, primary CNS lymphoma; PFS, progression-free survival; pMRI, perfusion MRI; rCBF, relative cerebral blood flow; rCBV, relative cerebral blood volume; TP, tumour progression; TRA, treatment-related abnormalities. [a]Optimal threshold value calculated from the available data from 190 individual patients. [b]Predefined, widely used threshold applied to the available data from 115 patients. [c]Threshold derived from own independent cohort ($n = 25$), range from literature. [d]Seven on glioma, three on brain metastasis. [e]Best-performing metric per study. [f,g]Meta-analyses that include some of the same studies.

glioma from primary CNS lymphoma (PCNSL)[74] (TABLE 2). Compared with high-grade glioma, PCNSL typically displayed lower values for several perfusion metrics, including rCBV. DSC was the most accurate (AUC 0.98) and sensitive (0.96, 95% CI 0.92–0.99) technique, but arterial spin labelling (ASL) was the most specific (0.90, 95% CI 0.78–0.96). Given its direct relationship with (neo)angiogenesis, pMRI has also been used to predict response to treatment with bevacizumab. A meta-analysis found an association between decreased (compared with pretreatment perfusion), or low, post-treatment perfusion and greater progression-free and overall survival[75] (TABLE 2).

Dynamic contrast-enhanced MRI. Dynamic contrast-enhanced (DCE) MRI is primarily used to assess the leakage of contrast agent through the blood–brain barrier (FIG. 2). In brain tumours, the blood-brain barrier is disrupted by neovascularization — these new, poorly developed vessels lack the tight junctions that normally maintain the blood–brain barrier — and/or dysregulation of pericytes, growth factor release and immune responses that directly affects the endothelial barrier[76]. The volume transfer constant (K^{trans}) is the most widely used DCE metric and provides an estimate of vessel permeability. The QIBA claim for K^{trans} in the brain is that a longitudinal change of ≥21.3% can be attributed to true change, as opposed to measurement error, with the caveat that this claim is based on very limited literature[77,78]. This limitation is illustrated in TABLE 2, which includes only a few DCE studies, preventing reliable quantitative analyses and/or determination of thresholds[79].

Arterial spin labelling. ASL provides a measure of cerebral blood flow (CBF), using inflowing blood as contrast, and thus does not require the administration of a contrast agent. Various implementations of ASL are available; however, the publication of consensus recommendations[80] has achieved some form of harmonization, most notably on the use of pseudocontinuous ASL with a 3D readout, which has now been implemented by all main MRI scanner vendors.

Although a QIBA committee on ASL has been installed, a QIBA profile or claim on ASL has not yet been published[81]. In a meta-analysis of nine studies, both absolute CBF and CBF ratios were found to be significantly increased in high-grade glioma compared with low-grade glioma[82] (TABLE 2). As ASL is non-invasive, the technique holds particular potential for use in the paediatric population. A meta-analysis of 14 studies in children with brain tumours found that ASL can be used to differentiate between high-grade and low-grade glioma with 83% accuracy, at a maximum CBF ratio threshold of 1.45 (with a range of 0.94–1.52 in the literature)[35] (TABLE 2). However, diffuse midline glioma was excluded from the analysis, as it had low CBF ratios, despite being a high-grade tumour. ASL has also been used to retrospectively predict *IDH* genotype in patients with newly diagnosed glioma ($n = 40$; sensitivity 0.75, specificity 0.88)[83] and glioblastoma ($n = 149$; AUC 0.68)[84].

Proton MRS

MRS in neuro-oncology is mostly used as a third-line diagnostic tool. Proton MRS is based on the principle that protons within different molecules have slightly different resonance frequencies and can thus be detected and quantified[85]. The two main MRS techniques are single voxel spectroscopy and MRS imaging (MRSI). The spatial resolution of MRSI is higher than that of single voxel spectroscopy, but remains poor in comparison with other advanced imaging techniques. The degree to which molecules can be detected with MRS depends on the applied scanning technique, which is as-yet not standardized. In 2019, a group of 49 experts from the International Society for Magnetic Resonance in Medicine MRS study group published a consensus statement[86] on clinical proton MRS of the brain, with the aim of improving the quality of future MRS studies, increasing standardization and recommending the best MRS implementation to the vendors of MRI scanners. This consensus statement contains guidance on how to perform MRS at various field strengths and for specific indications, as well as a strong recommendation towards automated analysis methods and quality assurance, which will move the MRS field towards more quantitative applications.

In routine neuro-oncological practice, the typical molecules of interest are *N*-acetyl aspartate (NAA), choline, lactate, lipids and creatine. NAA is a neurotransmitter (resonance frequency at 2.0 ppm) that is abundantly

present in neurons and is thus reduced in any process that destroys neurons, whether neoplastic or non-neoplastic[85]. Choline (resonance frequency at 3.2 ppm) is commonly referred to as 'choline-containing compounds' and is considered a precursor of acetylcholine, which is a cell membrane component[85]. Therefore, choline is considered a marker of cellular membrane turnover and is increased in neoplastic processes. Lactate (doublet resonance centred at 1.3 ppm) is not normally present in the brain[85] and is a marker of any anaerobic process, such as — even non-necrotic — lower-grade diffuse glioma, infections or abscesses. Lipids comprise mobile lipid resonances (broad methyl and methylene resonance frequencies at 0.9 and 1.3 ppm) and are metabolites associated with necrosis. As such, lipid concentrations are greater in high-grade tumours, such as glioblastoma, than in low-grade tumours, such as astrocytoma[85,87]. Creatine/phosphocreatine is usually present (resonance frequency at 3.0 ppm) in metabolically active tissue such as the brain. Creatine levels are relatively constant and thus are commonly used as an internal standard for calculating ratios[85]. Since the incorporation of *IDH* mutation status in glioma classification in 2016, the detection of 2-hydroxyglutarate (2-HG), an oncometabolite of *IDH*-mut glioma, has become of interest[88].

Common metabolites. A QIBA committee on MRS has not yet been formed, and thus a profile has not yet been published. The quantification of MRS-derived metabolites is not yet standardized and there are no uniformly accepted thresholds for specific indications in neuro-oncology. Nevertheless, in a study comparing metastases ($n = 25$) with high-grade glioma ($n = 31$), the presence of a creatine peak was associated with gliobastoma[89]. Additionally, in a prospective study in 60 participants, NAA/creatine and choline/creatine ratios were higher in metastasis than in glioma[90]. In an MRS study in 42 treatment-naive patients with a variety of brain tumour types, the apparent lipid concentration correlated with astrocytoma tumour grade[87]. Of all the metabolites measured in the study (myo-inositol, creatine, choline, lactate and lipids) the combined quantification of lipids and macromolecules (non-metabolite proteins in the brain) was the most useful single parameter for the determination of astrocytoma grade.

A meta-analysis of nine studies indicated that MRS can distinguish tumour progression from treatment-related abnormalities with high accuracy (sensitivity 91%, specificity 95%)[38] (TABLE 3). A separate meta-analysis including 178 participants from seven studies found that choline/creatine and choline/NAA ratios were significantly higher in areas of tumour progression than in areas of radiation injury[69] (TABLE 3). However, these findings might depend on the timing of imaging, as the choline and creatine concentrations in areas of radiation necrosis have been reported to vary over time, owing to early radiation-induced changes in inflammation and demyelination[91].

Oncometabolites. 2-HG is probably the closest to a true imaging biomarker in neuro-oncology, as it provides a direct, quantitative marker of *IDH* genotype in glioma[88]. One meta-analysis found a very high pooled sensitivity (95%) and specificity (91%) of 2-HG for differentiating *IDH*-mut from *IDH*-wt glioma[92] (TABLE 3). 2-HG MRS has also been used to assess response to treatment. In two longitudinal studies in 136 (REF.[81]) and 24 (REF.[82]) participants with *IDH*-mut tumours, 2-HG increased with tumour progression and decreased with treatment response; this result is of particular interest for the assessment of IDH-targeted treatments[93]. Other studies have shown that 2-HG levels correlate with tumour volume[94] and cellularity[94,95]. In a retrospective study in 82 patients with *IDH*-mut ($n = 11$) and *IDH*-wt ($n = 71$) glioblastoma, a false-positive rate of 21% was observed with 2-HG MRS-based diagnosis[96]. These false positives seemed to be associated with the presence of necrosis. 2-HG MRS is still very much in the research domain, requiring specialist sequences and post-processing techniques, and its detection is highly technique-dependent.

In 2019, the first use of oncometabolite MRS to identify to 1p/19q co-deletion was reported. The 1p/19q co-deletion results in the loss of two enzymes located on the short arm of chromosome 1, causing an accumulation

Table 3 | **Meta-analyses of MR spectroscopy studies in neuro-oncology**

Meta-analysis	Number of studies (number of participants)	Technique and metric	Threshold	AUC (95% CI)	Sensitivity (95% CI)	Specificity (95% CI)	Other
Distinguishing tumour progression from treatment-related abnormalities							
Chuang et al. (2016)[a,69]	Five on glioma, two on brain metastases (178: 113 TP and 65 TRA)	Choline/creatine ratio	1.79–3.07	NA	NA	NA	Significantly higher in tumour progression
		Choline/NAA ratio	1.32–3.48	NA	NA	NA	Significantly higher in tumour progression
van Dijken et al. (2017)[a,38]	9 (203 HGG)	MRS	NA	NA	91% (79–97%)	95% (65–99%)	NA
Detecting IDH mutation							
Suh et al. (2018)[92]	14 (461: 224 with and 237 without *IDH* mutation)	2-HG	Summary	0.96	0.95	0.91	NA
	5 (173: 106 with and 67 without *IDH* mutation)	2-HG	1.76 mM	NA	0.75	0.95	NA

2-HG, 2-hydroxyglutarate; AUC, area under the receiver operating characteristic curve; HGG, high-grade glioma; IDH, isocitrate dehydrogenase; MRS, magnetic resonance spectroscopy; NA, not available; NAA, *N*-acetyl aspartate; TP, tumour progression; TRA, treatment-related abnormalities. [a]Meta-analyses that include some of the same studies.

Deep learning
A class of machine learning based on artificial neural networks that are inspired by biological networks of learning and information processing; 'deep' refers to the use of multiple layers in the network.

Overfitting
A phenomenon that occurs when the match between the classification model and the data set is too perfect, resulting in a model that cannot be generalized to any other data set.

Dimensionality
The number of dimensions included in a computational model; in radiomics, this term relates primarily to the number of imaging features, each feature being one dimension.

Noise
The unexplained variation or randomness in a computational model.

of cystathionine that can be measured with a dedicated MRS analysis[97]. Similar to 2-HG, MRS techniques for detection of cystathionine are highly specialised and have yet to make their way from the research domain to clinical practice.

Radiomics

Radiomics is the rapidly evolving field of converting medical images into objective high-dimensional data that can be collected in, and shared through, large databases or repositories[98]. The aim of radiomics is to associate imaging phenotypes with clinically or biologically relevant characteristics of the disease or the patient. In contrast to imaging biomarkers, which are mostly used in isolation, radiomics is by definition based on the analysis of a multitude of imaging features, thereby improving diagnostic accuracy[99]. The term 'radiomic signature' is used to refer to the summary of radiomics features that is specific to a particular disease state. Radiomics uses automated computational techniques for image analysis, thus overcoming issues with inter-rater and technical variability. Compared with more traditional approaches, these computational techniques are better able to handle the increasing complexity of both imaging techniques and our understanding of tumour biology. Importantly, radiomics is not confined to a single imaging technique or modality, but is well suited to the amalgamation of multiple kinds of imaging data (for example, MRI and PET) for multiparametric and multimodal assessment.

Radiomics data can also be combined with 'omics' data from other disciplines. For example, radiogenomics combines radiomics and genomics data to predict the genotype of a tumour on the basis of its imaging phenotype. In the field of neuro-oncology, radiogenomics research has had a major boost from The Cancer Genome Atlas and The Cancer Imaging Archive initiatives, which provide a wealth of publicly available oncological data.

Manual annotation

One of the first studies to successfully identify an association between gene expression and MRI characteristics in glioblastoma used manual annotation of imaging features[100]. Probably the most widely used lexicon for manual annotation of glioma is the visually accessible Rembrandt images (VASARI) lexicon[101]. VASARI constitutes a set of 24 well-defined and neuroradiologically well-known descriptors of glioma on conventional MRI, has been used to annotate several data sets from The Cancer Imaging Archive, and was used in some of the first radiogenomics studies on glioblastoma[102]. The essential feature that distinguishes VASARI from routine tumour description, is the provision of a lexicon that has demonstrated high reproducibility amongst a large number of raters[101]. Later work indicated that VASARI features correlate well with computationally obtained imaging features in glioblastoma[103].

Computational feature extraction

With the advances in image analysis techniques, the manual process of feature extraction is being replaced by algorithms that are able to extract large numbers of features from an image automatically. Traditionally, these are predefined mathematical features that are selected independently from the data set. However, an alternative approach is to use deep learning techniques to discover meaningful features from the data set itself[104]. This agnostic approach allows a more powerful, data-driven feature discovery than traditional approaches but requires much larger imaging data sets because the features are highly correlated with the input data, resulting in a high risk of overfitting. With both approaches, it is crucial that the input data are representative, well balanced, and sufficiently heterogeneous to allow generalizability of findings to similar scenarios.

The radiomics pipeline. The traditional radiomics pipeline consists of the following steps[104–106]: image preprocessing, segmentation, feature extraction, classification and feature reduction (FIG. 3). During the preprocessing step, the imaging data are prepared for analysis, which includes the alignment of all available imaging types or modalities. During segmentation, the tumour is outlined and subregions of the tumour, called habitats, can also be defined. The imaging features are then extracted from these segmented region(s) before being correlated with the class label (for example, the presence or absence of *IDH* mutation). Typically, several hundred features are identified, many of which will be cross-correlated, redundant or irrelevant. Thus, in the final step, feature reduction is applied to reduce dimensionality and noise caused by unnecessary features, as well as to reduce the risk of overfitting.

Prediction modelling and validation. Once the appropriate set of features has been selected, a prediction model can be built using an approach such as logistic regression or machine learning[99]. To avoid overfitting, the model needs to be built with data that are not used to assess model performance. A common method is to split the data set into a larger 'training' set and smaller 'validation' set, to train and tune the model using a method such as cross-validation. The performance of the final model should then be determined using an independent, so-called 'test' set, consisting of data from an entirely different source that have not yet been 'seen' by the model.

Applications of radiomics

The application of machine learning and radiomics has yet to find its way into clinical neuro-oncological practice; however, these approaches have shown encouraging results for a variety of indications. Many studies have used radiomics, mostly with conventional MRI data, to investigate a variety of indications in glioma and other brain tumours[104,105]. However, the majority of such studies lacked appropriate validation and testing, so these results should be considered as exploratory and interpreted with caution.

In a meta-analysis of six studies, including a total of 440 participants, a form of radiomics known as MRI texture analysis had a high accuracy for the grading of glioma, with a pooled sensitivity of 0.93 (95% CI 0.88–0.96), a specificity of 0.86 (95% CI 0.81–0.89) and an AUC of

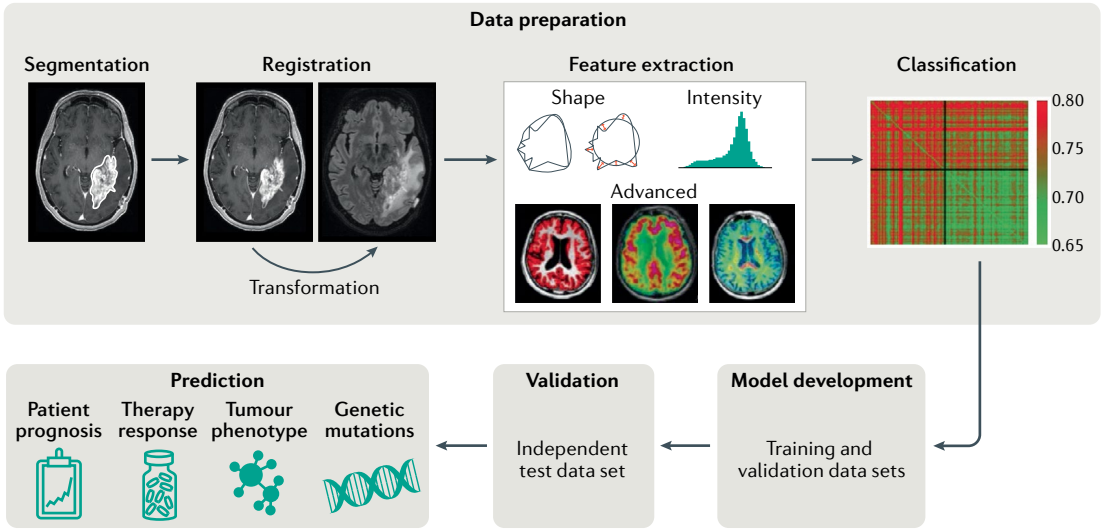

Fig. 3 | **Radiomics pipeline.** Radiomics pipelines begin with tumour segmentation and image alignment (registration), after which imaging features are extracted and classified. After feature reduction (not shown) the model is trained with a training data set and a validation data set. The resulting model is then externally validated using an independent test data set to determine its performance for the prediction of clinically relevant parameters. Figure adapted with permission from REF.[106], Elsevier.

0.96 (REF.[107]). In a single study in 113 participants, deep learning was applied to the grading of glioma from conventional MR images and achieved an accuracy of 95% in the validation data set[108]. Radiomics approaches have also been applied to the differentiation of tumour progression and treatment-related abnormalities such as radiation necrosis. A study in 95 participants used logistic regression to analyse multiparametric MRI data, including information from post-contrast T1-weighted and T2-weighted fluid-attenuated inversion recovery imaging, as well as ADC and rCBV maps[109,110]. The resulting model was able to identify radiation necrosis tissue with an AUC of 0.85. A deep learning approach using only post-contrast T1-weighted images for the same indication yielded a similar AUC of 0.83 in a study in 78 participants[111]. Furthermore, a study in 34 participants used PET radiomics to differentiate tumour progression from radiation necrosis with an AUC of 0.74 (REF.[112]).

Radiomics has also been tested as a method of determining patient prognosis. In several studies, each involving ~100 participants with newly diagnosed glioblastoma, radiomics analysis outperformed clinical and radiological models of patient survival[113–115]. In a study in 117 participants with lower-grade glioma, radiomics predicted survival as well as Ki-67 expression level with an accuracy of 89%[116]. Machine learning was also successfully used to map glioblastoma cellularity on the basis of 91 targeted biopsies from 36 patients[117]. Of note, almost none of the radiomics studies described in this section used a truly independent test data set, only a validation set consisting of a small portion of the overall cohort, limiting the generalizability of these results.

Radiogenomics of glioma. Given the recent insights into, as well as the clinical implications of, molecular classification of glioma, a large body of work has focused on the prediction of glioma genotype from imaging phenotypes. This approach is known as radiogenomics and one of the earliest studies in the field used a subset of the VASARI lexicon to predict the molecular profile of glioblastoma. Four gene expression classes were used: proneural, neural, classic and mesenchymal. Compared with the other subgroups, proneural glioblastoma had significantly less enhancement and mesenchymal glioblastoma had less non-enhancing tumour[102]. Another study found that four robust quantitative imaging features were significantly correlated with molecular subgroups of glioblastoma, and that three other imaging features correlated with survival[103]. A meta-analysis of visually assessable features identified preferential frontal lobe location, sharply demarcated borders, T2-FLAIR mismatch sign[118], higher ADC, lower FA and lower rCBV as characteristic of *IDH*-mut glioma[40,119].

In a study in 259 participants, a deep learning approach was used to classify genetic mutations in glioma from conventional MRI[120]. This approach predicted *IDH* genotype with an AUC of 0.94, 1p/19q co-deletion with an AUC of 0.92 and MGMT promotor methylation status with an AUC of 0.83. Conventional MRI radiomics was also able to identify high-risk glioblastoma[121]. In a systematic review of studies that used machine learning to predict *IDH* genotype (nine studies and a total of 996 participants), the pooled AUC was 0.89 (95% CI 0.86–0.92), the pooled sensitivity was 0.87 (95% CI 0.76–0.93) and the pooled specificity was 0.90 (95% CI 0.72–97)[122]. Of note, only five of the nine studies had divided their study population into a training set and a validation set, and none had externally validated their results in an independent test data set. A more recent systematic review of 14 studies in 1,655 participants with lower-grade glioma showed similar findings[123]: the best classifier of *IDH* genotype had an AUC of 0.95, 94.4% sensitivity and 86.7% specificity, and the best

Radiomics quality score
A score system used to assess the quality of radiomics studies; consists of 16 items covering methodology, reporting, clinical utility and contribution to open science.

classifier of 1p/19q co-deletion status had an AUC of 0.96, 90% sensitivity and 89% specificity[123]. However, the calculated radiomics quality score indicated that the overall clinical applicability of the studies included in the review was inadequate, identifying amongst other issues a lack of prospective validation[99,111]. Performance of radiogenomics techniques in studies with external validation is generally lower than in such unvalidated studies. For example, in a study using machine learning analysis of non-enhancing glioma, the AUC for prediction of 1p/19q co-deletion in an independent test data set was 0.72 (REF.[124]).

In addition to the prediction of such point mutations, attempts have also been made to predict the signalling pathways involved in glioma survival. For example, in a study combining patient cohorts from the Chinese Glioma Genome Atlas and The Cancer Genome Atlas, several radiomics features were found to be associated with both progression-free survival in lower-grade glioma and a specific set of genetic mutations, pointing towards the involvement of specific signalling pathways[125].

Radiomics in brain metastasis. In brain metastasis[126], studies have used radiomics to differentiate solitary metastases from glioblastoma (AUC 0.91)[127], metastases from underlying primary cancers (AUC 0.87)[128], and radiation necrosis from tumour progression (AUC 0.94)[129]. Radiomics has also been used for automated detection and segmentation of brain metastases[130–132].

Automated response assessment. Machine learning is also being explored for the automated assessment of treatment response. In a study focusing on volumetric tumour assessment, machine learning predicted patient outcome with a higher accuracy than manual assessment of scans according to RANO criteria[133]. Such an approach could improve accuracy and reduce the substantial manual labour burden involved in outcome assessment in clinical trials. Additionally, radiomics has the potential to surpass the current focus on tumour volume burden as the sole radiographic outcome parameter by also capturing the heterogeneous molecular and biological characteristics of the tumour's response to treatment.

Limitations

Similar to imaging biomarkers, independent clinical validation of radiomics applications is commonly lacking. In a review of >500 studies of artificial intelligence algorithms, only 6% had performed external validation[134]. In a more recent review of 51 original radiomics studies on glioma, 29% had performed external validation[135]. Only 2% of studies had conducted test–retest analysis and only 4% had a prospective study design. As a result, the vast majority of radiomics findings are not yet generalizable and reported performance is commonly over-optimistic.

Conclusions

From a historically qualitative discipline, radiology is in the process of transitioning into a quantitative science. Imaging biomarkers and radiomics are at the core this transformation, addressing the currently unmet need to answer questions regarding brain tumour biology, physiology and treatment response, while exploiting the wealth of information that can now be obtained from the imaging data. Novel MRI techniques — such as fast, quantitative T1 mapping and T2 mapping[136], and chemical exchange saturation transfer (CEST)[137] — are now on the horizon and could provide even more detailed tumour characterization. Additionally, techniques such as CEST and MRS benefit from acquisition at ultra-high field strength (7 T and higher)[138]. In neuro-oncology, the transition to quantitative imaging benefits from a multidisciplinary approach, such that advances in imaging technology and analysis are paired with anticipated novel treatments[20].

Although the various quantitative imaging parameters and radiomics hold much potential, considerable progress needs to be made before truly quantitative imaging approaches can be used in clinical practice. Despite the abundance of literature and widespread use of quantitative imaging in neuro-oncology, none of the existing metrics meet all imaging biomarker standards. The vast majority of published studies were small and retrospective, and the methods and metrics used varied widely among studies. None of the meta-analyses discussed in this Review were able to provide independently validated threshold values — common sources of heterogeneity were technical aspects (acquisition, analysis) and patient cohorts (selection, inclusion, size).

Variations in imaging acquisition and reconstruction, post-processing, and analysis are numerous, and some degree of harmonization will be essential to move the field forward, although some issues can be overcome by artificial intelligence-based solutions[139]. Important steps in the right direction have been made by the publication of consensus recommendations on MRI protocols for glioma[140] and brain metastasis[141], as well as on dMRI[78], ASL pMRI[80] and DSC pMRI[142]. An even more important impediment to the implementation of imaging biomarkers in clinical practice is the current lack of rigorous validation: only two quantitative imaging metrics (ADC and K^{trans}) have a QIBA claim on technical validity, the available research into imaging biomarkers is generally at the discovery level, and biological and clinical validation is largely absent.

The main radiological societies (ESR and RSNA) as well as independent organizations such as the Image Biomarker Standardisation Initiative (IBSI)[143] and the Open Source Initiative for Perfusion Imaging (OSIPI) are moving the field towards maturity by promoting use of consistent and correct terminology, and outlining qualification processes and standards. Uniformity in structuring, naming and annotating imaging data facilitates the pooling of multiple — clinically collected — data sets, such as in imaging biobanks or repositories[98,144]. This approach is further supported by the 'FAIR' principles that promote the findability, accessibility, interoperability and reuse of research data[145]. Biological validation can be improved by exploiting concurrent advances in histopathological data analysis techniques, enabling precise spatial correlation between MRI and histopathology[146]. Publicly available data sets such as The Cancer Imaging Archive can serve as independent test data sets for

technical validation. The annual Brain Tumor Image Segmentation (BRATS) challenge exemplifies how the image analysis community independently validates their algorithms[147]. Federated approaches, in which validation is done remotely, overcome issues with data transfer. Open access publication of not only results, but also of code and data, further supports technical validation. Finally, inequality of patient access to quantitative MRI requires attention, with a recent survey showing a worrying association between the use of quantitative MRI and gross domestic product within Europe[21].

Prospective clinical validation studies will be the final step to transition neuro-oncological imaging from current unidimensional markers of tumour burden to high-dimensional, complex biomarkers of tumour biology and response to treatment. These complex imaging biomarkers could, in combination with other non-invasive biomarkers, eventually serve as a 'virtual biopsy' for non-invasive precision diagnostics at every step of brain tumour management.

Published online 20 June 2021

1. Eckel-Passow, J. E. et al. Glioma groups based on 1p/19q, IDH, and TERT promoter mutations in tumors. *N. Engl. J. Med.* **372**, 2499–2508 (2015).
2. Louis, D. N. et al. WHO classification of tumours of the central nervous system. *Acta Neuropathol.* **131**, 803–820 (2016).
3. Suzuki, H. et al. Mutational landscape and clonal architecture in grade II and III gliomas. *Nat. Genet.* **47**, 458–468 (2015).
4. Wijnenga, M. M. J. et al. The impact of surgery in molecularly defined low-grade glioma: an integrated clinical, radiological, and molecular analysis. *Neuro Oncol.* **20**, 103–112 (2018).
5. Albert, N. L. et al. Response Assessment in Neuro-Oncology working group and European Association for Neuro-Oncology recommendations for the clinical use of PET imaging in gliomas. *Neuro Oncol.* **18**, 1199–1208 (2016).
6. Galldiks, N. et al. PET imaging in patients with meningioma–report of the RANO/PET Group. *Neuro Oncol.* **19**, 1576–1587 (2017).
7. Galldiks, N. et al. PET imaging in patients with brain metastasis–report of the RANO/PET group. *Neuro Oncol.* **21**, 585–595 (2019).
8. Kessler, L. G. et al. The emerging science of quantitative imaging biomarkers terminology and definitions for scientific studies and regulatory submissions. *Stat. Methods Med. Res.* **24**, 9–26 (2015).
Introduction to imaging biomarkers and associated terminology.
9. FDA-NIH Biomarker Working Group. *BEST (Biomarkers, EndpointS, and other Tools) Resource* (FDA, 2021).
10. O'Connor, J. P. et al. Imaging biomarker roadmap for cancer studies. *Nat. Rev. Clin. Oncol.* **14**, 169–186 (2017).
Outline and recommendations for development and introduction of imaging biomarkers for cancer.
11. Law, I. et al. Joint EANM/EANO/RANO practice guidelines/SNMMI procedure standards for imaging of gliomas using PET with radiolabelled amino acids and [^{18}F]FDG: version 1.0. *Eur. J. Nucl. Med. Mol. Imaging* **46**, 540–557 (2019).
12. Sullivan, D. C. et al. Metrology standards for quantitative imaging biomarkers. *Radiology* **277**, 813–825 (2015).
Introduction and outline of metrology in the context of imaging biomarkers.
13. deSouza, N. M. et al. Validated imaging biomarkers as decision-making tools in clinical trials and routine practice: current status and recommendations from the EIBALL* subcommittee of the European Society of Radiology (ESR). *Insights Imaging* **10**, 87 (2019).
14. Fournier, L. et al. Incorporating radiomics into clinical trials: expert consensus on considerations for data-driven compared to biologically driven quantitative biomarkers. *Eur. Radiol.* https://doi.org/10.1007/s00330-020-07598-8 (2021).
15. European Society of Radiology. ESR statement on the validation of imaging biomarkers. *Insights Imaging* **11**, 76 (2020).
16. European Medicines Agency. Guideline on bioanalytical method validation (EMA, 2011).
17. Alberich-Bayarri, A., Neri, E. & Martí-Bonmatí, L. in *Artificial Intelligence in Medical Imaging: Opportunities, Applications and Risks* Ch. 10 (eds Ranschaert, E. R., Morozov, S. & Algra, P. R.) 119–128 (Springer, 2019).
18. Obuchowski, N. A. et al. Statistical issues in testing conformance with the Quantitative Imaging Biomarker Alliance (QIBA) profile claims. *Acad. Radiol.* **23**, 496–506 (2016).
19. Huang, E. P. et al. Meta-analysis of the technical performance of an imaging procedure: guidelines and statistical methodology. *Stat. Methods Med. Res.* **24**, 141–174 (2015).
20. Yankeelov, T. E. et al. Quantitative imaging in cancer clinical trials. *Clin. Cancer Res.* **22**, 284–290 (2016).
21. Manfrini, E. et al. From research to clinical practice: a European neuroradiological survey on quantitative advanced MRI implementation. *Eur. Radiol.* https://doi.org/10.1007/s00330-020-07582-2 (2021).
22. Thust, S. C. et al. Glioma imaging in Europe: a survey of 220 centres and recommendations for best clinical practice. *Eur. Radiol.* **28**, 3306–3317 (2018).
23. Erker, C. et al. Response assessment in paediatric high-grade glioma: recommendations from the Response Assessment in Pediatric Neuro-Oncology (RAPNO) working group. *Lancet Oncol.* **21**, e317–e329 (2020).
24. Cha, S. Update on brain tumor imaging: from anatomy to physiology. *AJNR* **27**, 475–487 (2006).
25. Sugahara, T. et al. Usefulness of diffusion-weighted MRI with echo-planar technique in the evaluation of cellularity in gliomas. *J. Magn. Reson. Imaging* **9**, 53–60 (1999).
26. Higano, S. et al. Malignant astrocytic tumors: clinical importance of apparent diffusion coefficient in prediction of grade and prognosis. *Radiology* **241**, 839–846 (2006).
27. Quantitative Imaging Biomarkers Alliance. QIBA Profile: Diffusion-weighted magnetic resonance imaging (DWI). Profile consensus (QIBA, 2019).
28. Bonekamp, D. et al. Diffusion tensor imaging in children and adolescents: reproducibility, hemispheric, and age-related differences. *Neuroimage* **34**, 733–742 (2007).
29. Paldino, M. J., Barboriak, D., Desjardins, A., Friedman, H. S. & Vredenburgh, J. J. Repeatability of quantitative parameters derived from diffusion tensor imaging in patients with glioblastoma multiforme. *J. Magn. Reson. Imaging* **29**, 1199–1205 (2009).
30. Pfefferbaum, A., Adalsteinsson, E. & Sullivan, E. V. Replicability of diffusion tensor imaging measurements of fractional anisotropy and trace in brain. *J. Magn. Reson. Imaging* **18**, 427–433 (2003).
31. Sanvito, F., Castellano, A. & Falini, A. Advancements in neuroimaging to unravel biological and molecular features of brain tumors. *Cancers* **13**, 424 (2021).
32. Aliotta, E. et al. Automated apparent diffusion coefficient analysis for genotype prediction in lower grade glioma: association with the T2-FLAIR mismatch sign. *J. Neurooncol.* **149**, 325–335 (2020).
33. Zhang, L. et al. The utility of diffusion MRI with quantitative ADC measurements for differentiating high-grade from low-grade cerebral gliomas: evidence from a meta-analysis. *J. Neurol. Sci.* **373**, 9–15 (2017).
34. Wang, Q. P., Lei, D. Q., Yuan, Y. & Xiong, N. X. Accuracy of ADC derived from DWI for differentiating high-grade from low-grade gliomas: systematic review and meta-analysis. *Medicine* **99**, e19254 (2020).
35. Hales, P. W. et al. Arterial spin labelling and diffusion-weighted imaging in paediatric brain tumours. *Neuroimage Clin.* **22**, 101696 (2019).
36. Suh, C. H., Kim, H. S., Jung, S. C. & Kim, S. J. Diffusion-weighted imaging and diffusion tensor imaging for differentiating high-grade glioma from solitary brain metastasis: a systematic review and meta-analysis. *AJNR* **39**, 1208–1214 (2018).
37. Yu, Y. et al. Meta-analysis of the diagnostic performance of diffusion magnetic resonance imaging with apparent diffusion coefficient measurements for differentiating glioma recurrence from pseudoprogression. *Medicine* **99**, e20270 (2020).
38. van Dijken, B. R. J., van Laar, P. J., Holtman, G. A. & van der Hoorn, A. Diagnostic accuracy of magnetic resonance imaging techniques for treatment response evaluation in patients with high-grade glioma, a systematic review and meta-analysis. *Eur. Radiol.* **27**, 4129–4144 (2017).
39. Zulfiqar, M., Yousem, D. M. & Lai, H. ADC values and prognosis of malignant astrocytomas: does lower ADC predict a worse prognosis independent of grade of tumor?–a meta-analysis. *Am. J. Roentgenol.* **200**, 624–629 (2013).
40. Suh, C. H., Kim, H. S., Jung, S. C., Choi, C. G. & Kim, S. J. Imaging prediction of isocitrate dehydrogenase (IDH) mutation in patients with glioma: a systemic review and meta-analysis. *Eur. Radiol.* **29**, 745–758 (2019).
41. Aboian, M. S. et al. Imaging characteristics of pediatric diffuse midline gliomas with histone H3 K27M mutation. *AJNR* **38**, 795–800 (2017).
42. Poussaint, T. Y. et al. Apparent diffusion coefficient histogram metrics correlate with survival in diffuse intrinsic pontine glioma: a report from the Pediatric Brain Tumor Consortium. *Neuro Oncol.* **18**, 725–734 (2016).
43. Lober, R. M. et al. Diffusion-weighted MRI derived apparent diffusion coefficient identifies prognostically distinct subgroups of pediatric diffuse intrinsic pontine glioma. *J. Neurooncol.* **117**, 175–182 (2014).
44. Tan, W. L. et al. Can diffusion tensor imaging noninvasively detect IDH1 gene mutations in astrogliomas? A retrospective study of 112 cases. *AJNR* **35**, 920–927 (2014).
45. Aliotta, E. et al. Molecular subtype classification in lower-grade glioma with accelerated DTI. *AJNR* **40**, 1458–1463 (2019).
46. Miloushev, V. Z., Chow, D. S. & Filippi, C. G. Meta-analysis of diffusion metrics for the prediction of tumor grade in gliomas. *AJNR* **36**, 302–308 (2015).
47. Jiang, R. et al. The value of diffusion tensor imaging in differentiating high-grade gliomas from brain metastases: a systematic review and meta-analysis. *PLoS ONE* **9**, e112550 (2014).
48. Abdalla, G. et al. The diagnostic role of diffusional kurtosis imaging in glioma grading and differentiation of gliomas from other intra-axial brain tumours: a systematic review with critical appraisal and meta-analysis. *Neuroradiology* **62**, 791–802 (2020).
49. Zhang, H., Schneider, T., Wheeler-Kingshott, C. A. & Alexander, D. C. NODDI: practical in vivo neurite orientation dispersion and density imaging of the human brain. *Neuroimage* **61**, 1000–1016 (2012).
50. Panagiotaki, E. et al. Noninvasive quantification of solid tumor microstructure using VERDICT MRI. *Cancer Res.* **74**, 1902–1912 (2014).
51. Zaccagna, F. et al. Non-invasive assessment of glioma microstructure using VERDICT MRI: correlation with histology. *Eur. Radiol.* **29**, 5559–5566 (2019).
52. Le Bihan, D. et al. MR imaging of intravoxel incoherent motions: application to diffusion and perfusion in neurologic disorders. *Radiology* **161**, 401–407 (1986).
53. Falk Delgado, A., Nilsson, M., van Westen, D. & Falk Delgado, A. Glioma grade discrimination with MR diffusion kurtosis imaging: a meta-analysis of diagnostic accuracy. *Radiology* **287**, 119–127 (2018).
54. Li, W. F. et al. An evidence-based approach to assess the accuracy of intravoxel incoherent motion imaging for the grading of brain tumors. *Medicine* **97**, e13217 (2018).
55. Kadota, Y. et al. Differentiation between glioblastoma and solitary brain metastasis using neurite orientation dispersion and density imaging. *J. Neuroradiol.* **47**, 197–202 (2020).

56. Lefranc, M. et al. Perfusion MRI as a neurosurgical tool for improved targeting in stereotactic tumor biopsies. *Stereotact. Funct. Neurosurg.* **90**, 240–247 (2012).
57. Chakhoyan, A. et al. Validation of vessel size imaging (VSI) in high-grade human gliomas using magnetic resonance imaging, image-guided biopsies, and quantitative immunohistochemistry. *Sci. Rep.* **9**, 2846 (2019).
58. Smits, M. et al. Repeatability and reproducibility of relative cerebral blood volume measurement of recurrent glioma in a multicentre trial setting. *Eur. J. Cancer* **114**, 89–96 (2019).
59. Shin, W. et al. Quantitative cerebral perfusion using dynamic susceptibility contrast MRI: evaluation of reproducibility and age- and gender-dependence with fully automatic image postprocessing algorithm. *Magn. Reson. Med.* **58**, 1232–1241 (2007).
60. Caseiras, G. B. et al. Relative cerebral blood volume measurements of low-grade gliomas predict patient outcome in a multi-institution setting. *Eur. J. Radiol.* **73**, 215–220 (2010).
61. Jafari-Khouzani, K. et al. Repeatability of cerebral perfusion using dynamic susceptibility contrast MRI in glioblastoma patients. *Transl. Oncol.* **8**, 137–146 (2015).
62. Bell, L. C. et al. Evaluating multisite rCBV consistency from DSC-MRI imaging protocols and postprocessing software across the NCI quantitative imaging network sites using a digital reference object (DRO). *Tomography* **5**, 110–117 (2019).
63. Milchenko, M. V. et al. Comparison of perfusion- and diffusion-weighted imaging parameters in brain tumor studies processed using different software platforms. *Acad. Radiol.* **21**, 1294–1303 (2014).
64. Orsingher, L., Piccinini, S. & Crisi, G. Differences in dynamic susceptibility contrast MR perfusion maps generated by different methods implemented in commercial software. *J. Comput. Assist. Tomogr.* **38**, 647–654 (2014).
65. Quantitative Imaging Biomarkers Alliance. QIBA Profile: Dynamic susceptibility contrast MRI (DSC-MRI). Stage 2: Consensus profile (QIBA, 2020).
66. Delgado, A. F. & Delgado, A. F. Discrimination between glioma grades II and III using dynamic susceptibility perfusion MRI: a meta-analysis. *AJNR* **38**, 1348–1355 (2017).
67. Abrigo, J. M. et al. Magnetic resonance perfusion for differentiating low-grade from high-grade gliomas at first presentation. *Cochrane Database Syst. Rev.* **1**, CD011551 (2018).
68. Xing, Z. et al. Noninvasive assessment of IDH mutational status in World Health Organization grade II and III astrocytomas using DWI and DSC-PWI combined with conventional MR imaging. *AJNR* **38**, 1138–1144 (2017).
69. Chuang, M. T., Liu, Y. S., Tsai, Y. S., Chen, Y. C. & Wang, C. K. Differentiating radiation-induced necrosis from recurrent brain tumor using MR perfusion and spectroscopy: a meta-analysis. *PLoS ONE* **11**, e0141438 (2016).
70. Wang, L. et al. Evaluation of perfusion MRI value for tumor progression assessment after glioma radiotherapy: a systematic review and meta-analysis. *Medicine* **99**, e23766 (2020).
71. Patel, P. et al. MR perfusion-weighted imaging in the evaluation of high-grade gliomas after treatment: a systematic review and meta-analysis. *Neuro Oncol.* **19**, 118–127 (2017).
72. Smits, M. Imaging of oligodendroglioma. *Br. J. Radiol.* **89**, 1060 (2016).
73. Suh, C. H., Kim, H. S., Jung, S. C., Choi, C. G. & Kim, S. J. Perfusion MRI as a diagnostic biomarker for differentiating glioma from brain metastasis: a systematic review and meta-analysis. *Eur. Radiol.* **28**, 3819–3831 (2018).
74. Xu, W., Wang, Q., Shao, A., Xu, B. & Zhang, J. The performance of MR perfusion-weighted imaging for the differentiation of high-grade glioma from primary central nervous system lymphoma: a systematic review and meta-analysis. *PLoS ONE* **12**, e0173430 (2017).
75. Choi, S. H. et al. Perfusion MRI as the predictive/prognostic and pharmacodynamic biomarkers in recurrent malignant glioma treated with bevacizumab: a systematic review and a time-to-event meta-analysis. *J. Neurooncol.* **128**, 185–194 (2016).
76. Hoque, M. M. et al. The cerebral microvasculature: basic and clinical perspectives on stroke and glioma. *Microcirculation* **28**, e12671 (2021).
77. Quantitative Imaging Biomarkers Alliance. QIBA Profile: DCE-MRI Quantification (DCEMRI-Q). Stage 1: public comment (QIBA, 2017).
78. Shukla-Dave, A. et al. Quantitative Imaging Biomarkers Alliance (QIBA) recommendations for improved precision of DWI and DCE-MRI derived biomarkers in multicenter oncology trials. *J. Magn. Reson. Imaging* **49**, e101–e121 (2019).
79. Okuchi, S. et al. Diagnostic accuracy of dynamic contrast-enhanced perfusion MRI in stratifying gliomas: a systematic review and meta-analysis. *Cancer Med.* **8**, 5564–5573 (2019).
80. Alsop, D. C. et al. Recommended implementation of arterial spin-labeled perfusion MRI for clinical applications: a consensus of the ISMRM perfusion study group and the European consortium for ASL in dementia. *Magnetic Reson. Med.* **73**, 102–116 (2015).
81. Quantitative Imaging Biomarkers Alliance. EIBIR/QIBA ASL Biomarker Committee (QIBA, 2019).
82. Kong, L., Chen, H., Yang, Y. & Chen, L. A meta-analysis of arterial spin labelling perfusion values for the prediction of glioma grade. *Clin. Radiol.* **72**, 255–261 (2017).
83. Brendle, C. et al. Glioma grading and determination of IDH mutation status and ATRX loss by DCE and ASL perfusion. *Clin. Neuroradiol.* **28**, 421–428 (2018).
84. Yoo, R. E. et al. Arterial spin labeling perfusion-weighted imaging aids in prediction of molecular biomarkers and survival in glioblastomas. *Eur. Radiol.* **30**, 1202–1211 (2020).
85. Bertholdo, D., Watcharakorn, A. & Castillo, M. Brain proton magnetic resonance spectroscopy: introduction and overview. *Neuroimaging Clin. N. Am.* **23**, 359–380 (2013).
86. Wilson, M. et al. Methodological consensus on clinical proton MRS of the brain: review and recommendations. *Magn. Reson. Med.* **82**, 527–550 (2019).
87. Howe, F. A. et al. Metabolic profiles of human brain tumors using quantitative in vivo 1H magnetic resonance spectroscopy. *Magn. Reson. Med.* **49**, 223–232 (2003).
88. Choi, C. et al. 2-hydroxyglutarate detection by magnetic resonance spectroscopy in IDH-mutated patients with gliomas. *Nat. Med.* **18**, 624–629 (2012).
89. Ishimaru, H. et al. Differentiation between high-grade glioma and metastatic brain tumor using single-voxel proton MR spectroscopy. *Eur. Radiol.* **11**, 1784–1791 (2001).
90. Caivano, R. et al. 3 Tesla magnetic resonance spectroscopy: cerebral gliomas vs. metastatic brain tumors. Our experience and review of the literature. *Int. J. Neurosci.* **123**, 537–543 (2013).
91. Esteve, F., Rubin, C., Grand, S., Kolodie, H. & Le Bas, J. F. Transient metabolic changes observed with proton MR spectroscopy in normal human brain after radiation therapy. *Int. J. Radiat. Oncol. Biol. Phys.* **40**, 279–286 (1998).
92. Suh, C. H., Kim, H. S., Jung, S. C., Choi, C. G. & Kim, S. J. 2-Hydroxyglutarate MR spectroscopy for prediction of isocitrate dehydrogenase mutant glioma: a systemic review and meta-analysis using individual patient data. *Neuro Oncol.* **20**, 1573–1583 (2018).
93. Andronesi, O. C. et al. Treatment response assessment in IDH-mutant glioma patients by noninvasive 3D functional spectroscopic mapping of 2-hydroxyglutarate. *Clin. Cancer Res.* **22**, 1632–1641 (2016).
94. de la Fuente, M. I. et al. Integration of 2-hydroxyglutarate-proton magnetic resonance spectroscopy into clinical practice for disease monitoring in isocitrate dehydrogenase-mutant glioma. *Neuro Oncol.* **18**, 283–290 (2016).
95. Choi, C. et al. Prospective longitudinal analysis of 2-hydroxyglutarate magnetic resonance spectroscopy identifies broad clinical utility for the management of patients with IDH-mutant glioma. *J. Clin. Oncol.* **34**, 4030–4039 (2016).
96. Suh, C. H. et al. False-positive measurement at 2-hydroxyglutarate MR spectroscopy in isocitrate dehydrogenase wild-type glioblastoma: a multifactorial analysis. *Radiology* **291**, 752–762 (2019).
97. Branzoli, F. et al. Cystathionine as a marker for 1p/19q codeleted gliomas by in vivo magnetic resonance spectroscopy. *Neuro Oncol.* **21**, 765–774 (2019).
98. Gillies, R. J., Kinahan, P. E. & Hricak, H. Radiomics: images are more than pictures, they are data. *Radiology* **278**, 563–577 (2016).
Introduction to radiomics.
99. Lambin, P. et al. Radiomics: the bridge between medical imaging and personalized medicine. *Nat. Rev. Clin. Oncol.* **14**, 749–762 (2017).
Quality standards for radiomics studies.
100. Diehn, M. et al. Identification of noninvasive imaging surrogates for brain tumor gene-expression modules. *Proc. Natl Acad. Sci. USA* **105**, 5213–5218 (2008).
101. TCGA Glioma Phenotpye Research Group. VASARI research project. *Cancer Imaging Archive* https://wiki.cancerimagingarchive.net/display/Public/VASARI+Research+Project (2020)
102. Gutman, D. A. et al. MR imaging predictors of molecular profile and survival: multi-institutional study of the TCGA glioblastoma data set. *Radiology* **267**, 560–569 (2013).
103. Gevaert, O. et al. Glioblastoma multiforme: exploratory radiogenomic analysis by using quantitative image features. *Radiology* **273**, 168–174 (2014).
104. Lohmann, P. et al. Radiomics in neuro-oncology: basics, workflow, and applications. *Methods* **188**, 112–121 (2020).
Comprehensive overview and explanation of radiomics.
105. Rudie, J. D., Rauschecker, A. M., Bryan, R. N., Davatzikos, C. & Mohan, S. Emerging applications of artificial intelligence in neuro-oncology. *Radiology* **290**, 607–618 (2019).
Overview of applications of radiomics and other computational methods in neuro-oncological imaging.
106. Starmans, M. P. A. et al. in *Handbook of Medical Image Computing and Computer Assisted Intervention* (eds Zhou, S. K., Rueckert, D. & Fichtinger, G.) 429–456 (Academic, 2020).
107. Wang, Q., Lei, D., Yuan, Y. & Zhao, H. Accuracy of magnetic resonance imaging texture analysis in differentiating low-grade from high-grade gliomas: systematic review and meta-analysis. *BMJ Open* **9**, e027144 (2019).
108. Yang, Y. et al. Glioma grading on conventional MR images: a deep learning study with transfer learning. *Front. Neurosci.* **12**, 804 (2018).
109. Kim, J. Y. et al. Incorporating diffusion- and perfusion-weighted MRI into a radiomics model improves diagnostic performance for pseudoprogression in glioblastoma patients. *Neuro Oncol.* **21**, 404–414 (2019).
110. Hu, X., Wong, K. K., Young, G. S., Guo, L. & Wong, S. T. Support vector machine multiparametric MRI identification of pseudoprogression from tumor recurrence in patients with resected glioblastoma. *J. Magn. Reson. Imaging* **33**, 296–305 (2011).
111. Jang, B. S., Jeon, S. H., Kim, I. H. & Kim, I. A. Prediction of pseudoprogression versus progression using machine learning algorithm in glioblastoma. *Sci. Rep.* **8**, 12516 (2018).
112. Lohmann, P. et al. FET PET radiomics for differentiating pseudoprogression from early tumor progression in glioma patients post-chemoradiation. *Cancers* **12**, 3835 (2020).
113. Kickingereder, P. et al. Radiomic profiling of glioblastoma: identifying an imaging predictor of patient survival with improved performance over established clinical and radiologic risk models. *Radiology* **280**, 880–889 (2016).
114. Macyszyn, L. et al. Imaging patterns predict patient survival and molecular subtype in glioblastoma via machine learning techniques. *Neuro Oncol.* **18**, 417–425 (2016).
115. Li, Q. et al. A fully-automatic multiparametric radiomics model: towards reproducible and prognostic imaging signature for prediction of overall survival in glioblastoma multiforme. *Sci. Rep.* **7**, 14331 (2017).
116. Li, Y. et al. Radiomic features predict Ki-67 expression level and survival in lower grade gliomas. *J. Neurooncol.* **135**, 317–324 (2017).
117. Chang, P. D. et al. A multiparametric model for mapping cellularity in glioblastoma using radiographically localized biopsies. *AJNR* **38**, 890–898 (2017).
118. Goyal, A. et al. The T2-FLAIR-mismatch sign as an imaging biomarker for IDH and 1p/19q status in diffuse low-grade gliomas: a systematic review with a Bayesian approach to evaluation of diagnostic test performance. *Neurosurg. Focus.* **47**, E13 (2019).
119. Smits, M. & van den Bent, M. J. Imaging correlates of adult glioma genotypes. *Radiology* **284**, 316–331 (2017).
120. Chang, P. et al. Deep-learning convolutional neural networks accurately classify genetic mutations in gliomas. *AJNR* **39**, 1201–1207 (2018).
121. Verma, R. et al. tumor habitat-derived radiomic features at pretreatment MRI that are prognostic for progression-free survival in glioblastoma are associated with key morphologic attributes at

histopathologic examination: a feasibility study. *Radiol. Artif. Intell.* **2**, e190168 (2020).
122. Zhao, J. et al. Diagnostic accuracy and potential covariates for machine learning to identify IDH mutations in glioma patients: evidence from a meta-analysis. *Eur. Radiol.* **30**, 4664–4674 (2020).
123. Bhandari, A. P., Liong, R., Koppen, J., Murthy, S. V. & Lasocki, A. Noninvasive determination of IDH and 1p19q status of lower-grade gliomas using MRI radiomics: a systematic review. *AJNR* **42**, 94–101 (2021).
124. van der Voort, S. R. et al. Predicting the 1p/19q codeletion status of presumed low-grade glioma with an externally validated machine learning algorithm. *Clin. Cancer Res.* **25**, 7455–7462 (2019).
125. Liu, X. et al. A radiomic signature as a non-invasive predictor of progression-free survival in patients with lower-grade gliomas. *Neuroimage Clin.* **20**, 1070–1077 (2018).
126. Tong, E., McCullagh, K. L. & Iv, M. Advanced imaging of brain metastases: from augmenting visualization and improving diagnosis to evaluating treatment response. *Front. Neurol.* **11**, 270 (2020).
127. Petrujkic, K. et al. Computational quantitative MR image features – a potential useful tool in differentiating glioblastoma from solitary brain metastasis. *Eur. J. Radiol.* **119**, 108634 (2019).
128. Ortiz-Ramon, R., Larroza, A., Ruiz-Espana, S., Arana, E. & Moratal, D. Classifying brain metastases by their primary site of origin using a radiomics approach based on texture analysis: a feasibility study. *Eur. Radiol.* **28**, 4514–4523 (2018).
129. Larroza, A. et al. Support vector machine classification of brain metastasis and radiation necrosis based on texture analysis in MRI. *J. Magn. Reson. Imaging* **42**, 1362–1368 (2015).
130. Charron, O. et al. Automatic detection and segmentation of brain metastases on multimodal MR images with a deep convolutional neural network. *Comput. Biol. Med.* **95**, 43–54 (2018).
131. Liu, Y. et al. A deep convolutional neural network-based automatic delineation strategy for multiple brain metastases stereotactic radiosurgery. *PLoS ONE* **12**, e0185844 (2017).
132. Liu, Y. et al. Automatic metastatic brain tumor segmentation for stereotactic radiosurgery applications. *Phys. Med. Biol.* **61**, 8440–8461 (2016).
133. Kickingereder, P. et al. Automated quantitative tumour response assessment of MRI in neuro-oncology with artificial neural networks: a multicentre, retrospective study. *Lancet Oncol.* **20**, 728–740 (2019).
134. Kim, D. W., Jang, H. Y., Kim, K. W., Shin, Y. & Park, S. H. Design characteristics of studies reporting the performance of artificial intelligence algorithms for diagnostic analysis of medical images: results from recently published papers. *Korean J. Radiol.* **20**, 405–410 (2019).
135. Park, J. E. et al. A systematic review reporting quality of radiomics research in neuro-oncology: toward clinical utility and quality improvement using high-dimensional imaging features. *BMC Cancer* **20**, 29 (2020).
136. Ma, D. et al. Magnetic resonance fingerprinting. *Nature* **495**, 187–192 (2013).
137. Zhou, J., Heo, H. Y., Knutsson, L., van Zijl, P. C. M. & Jiang, S. APT-weighted MRI: techniques, current neuro applications, and challenging issues. *J. Magn. Reson. Imaging* **50**, 347–364 (2019).
138. Ladd, M. E. et al. Pros and cons of ultra-high-field MRI/MRS for human application. *Prog. Nucl. Magn. Reson. Spectrosc.* **109**, 1–50 (2018).
139. Carre, A. et al. Standardization of brain MR images across machines and protocols: bridging the gap for MRI-based radiomics. *Sci. Rep.* **10**, 12340 (2020).
140. Ellingson, B. M. et al. Consensus recommendations for a standardized Brain Tumor Imaging Protocol in clinical trials. *Neuro Oncol.* **17**, 1188–1198 (2015).
141. Kaufmann, T. J. et al. Consensus recommendations for a standardized brain tumor imaging protocol for clinical trials in brain metastases. *Neuro Oncol.* **22**, 757–772 (2020).
142. Boxerman, J. L. et al. Consensus recommendations for a dynamic susceptibility contrast MRI protocol for use in high-grade gliomas. *Neuro Oncol.* **22**, 1262–1275 (2020).
143. Zwanenburg, A. et al. The image biomarker standardization initiative: standardized quantitative radiomics for high-throughput image-based phenotyping. *Radiology* **295**, 328–338 (2020).
144. European Society of Radiology. ESR position paper on imaging biobanks. *Insights Imaging* **6**, 403–410 (2015).
145. Wilkinson, M. D. et al. The FAIR Guiding Principles for scientific data management and stewardship. *Sci. Data* **3**, 160018 (2016).
146. Al-Mubarak, H. et al. Stacked in-plane histology for quantitative validation of non-invasive imaging biomarkers: application to an infiltrative brain tumour model. *J. Neurosci. Methods* **326**, 108372 (2019).
147. Bakas, S. et al. Advancing The Cancer Genome Atlas glioma MRI collections with expert segmentation labels and radiomic features. *Sci. Data* **4**, 170117 (2017).

Competing interests
M.S. declares speaker fees paid to her institution from GE Healthcare and honorarium paid to her institution from Parexel Ltd. for trial review of EORTC-1410.

Peer review information
Nature Reviews Neurology thanks A. Waldman, who co-reviewed with G. Thompson, and the other, anonymous, reviewer(s) for their contribution to the peer review of this work.

Publisher's note
Springer Nature remains neutral with regard to jurisdictional claims in published maps and institutional affiliations.

RELATED LINKS
European Imaging Biomarkers Alliance (EIBALL): https://www.myesr.org/research/esr-research-committee
Open Source Initiative for Perfusion Imaging (OSIPI): https://www.osipi.org
Quantitative Imagine Biomarkers Alliance (QIBA): https://www.rsna.org/research/quantitative-imaging-biomarkers-alliance
Quantitative Imaging Biomarkers Alliance (QIBA) wiki: https://qibawiki.rsna.org/index.php/Main_Page
The Cancer Genome Atlas: https://www.cancer.gov/about-nci/organization/ccg/research/structural-genomics/tcga
The Cancer Imaging Archive: https://www.cancerimagingarchive.net